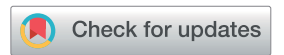
Journal of Materials Chemistry A



COMMUNICATION

View Article Online
View Journal | View Issue



Cite this: J. Mater. Chem. A, 2018, 6, 19941

Received 15th September 2018 Accepted 21st September 2018

DOI: 10.1039/c8ta08975b

rsc.li/materials-a

Improved stability and high thermoelectric performance through cation site doping in n-type La-doped Mg₃Sb_{1.5}Bi_{0.5}†

Kazuki Imasato, D * Max Wood, D Jimmy Jiahong Kuo D and G. Jeffrey Snyder D *

n-Type conduction in a ${\rm Mg_3Sb_{1.5}Bi_{0.5}}$ system is achieved with Ladoping at cation sites with a peak zT > 1. La-doped samples exhibit much higher doping efficiency and dopability compared to other chalcogen-doped samples. This allows greater tunability of the electronic properties. La-doping also significantly improves the thermal stability of n-type ${\rm Mg_3Sb_{1.5}Bi_{0.5}}$ measured via a long-term Hall carrier concentration measurement.

The n-type Mg_3Sb_2 – Mg_3Bi_2 alloy can be an exceptionally efficient thermoelectric material because of its highly degenerate conduction band and extremely low lattice thermal conductivity. The crystal structure of Mg_3Sb_2 can be thought of in terms of the $CaAl_2Si_2$ structure (space group $P\bar{3}m1$), which consists of an octahedrally coordinated Mg^{2+} cation layer and a tetrahedrally coordinated anion structure $(Mg_2Sb_2)^{2-}$. Long known to be an adequate p-type material through different optimization routes $^{5-8}$ ($zT\approx 0.7$), band structure calculations on Mg_3Sb_2 had shown its n-type properties to be superior. Attempts to dope the n-type material had failed until recently, when chalcogen (Te, Se, S) doped n-type materials were discovered by different research groups $^{1-3,10-15}$ and exhibited a promising zT value of ~ 1.5 at 750 K when alloyed with 25% Mg_3Bi_2 .

Initially, attempts to realize n-type conduction had failed due to charge compensating vacancy type defects at the cation site $(V_{Mg^{2-}})$. Once an appreciation of the importance of these charge compensating defects and their formation energies were realized, 1,16,17 their carrier concentrations were controlled through a process called phase boundary mapping. In the Mg_3Sb_2 system, there are two distinct thermodynamic states where materials could realistically be synthesized; a Mg-excess state and an Sb-excess state where the Mg_3Sb_2 matrix is in equilibrium with elemental Mg or Sb, respectively. n-Type conduction

 $\label{lem:prop:condition} Department of Materials Science and Engineering, Northwestern University, Evanston, IL 60208, USA. E-mail: jeff.snyder@northwestern.edu$

† Electronic supplementary information (ESI) available. See DOI: 10.1039/c8ta08975b

in Mg₃Sb₂-compounds is only attainable when the materials are synthesized in the Mg-excess state because the atomic chemical potential in the Mg excess state suppresses the formation of cation vacancies.^{3,17,18} In these high thermoelectric performance n-type materials, extrinsic dopants provide the conduction electrons as opposed to Mg interstitial atoms³ – the suppression of cation vacancies should enable a soluble donor dopant to produce n-type materials.

In addition to controlling the charge compensating defects, previous studies revealed that the limits of achievable carrier concentration varied depending on the type of electron donating defect that was chosen. Mg₃Sb_{1.5}Bi_{0.5} n-type materials have been synthesized with chalcogen (S, Se, Te) dopants, with S and Se failing to achieve optimal levels of carrier concentration. Additionally, chalcogen-doped Mg₃Sb_{1.5}Bi_{0.5} suffers from high temperature stability issues, which can be observed as a hysteresis or degradation of the n-type carrier concentration with multiple thermal cycles from testing. Pinally, chalcogen doped samples have a relatively low doping efficiency, with Te doped samples reaching a carrier concentration of only approximately 40% of the nominal dopant concentration (expecting 1e⁻ per Te atom) in an optimally doped sample.

Substituting the Group 2 Mg atoms with Group 3 elements is a plausible way to dope this alloy by donating one electron for each dopant atom to provide the necessary charge carrier concentration and the materials are predicted to be stable.²⁰ Doping the Mg site might have a more pronounced effect on the intrinsic electrical properties than doping the Sb site since the characteristics of the conduction band largely originate from Mg orbitals.^{2,9,21} In this study, we have investigated the effect of La-doping on the thermoelectric properties. Based on first principles calculations,²⁰ La was predicted to be a more effective dopant of the cation site for controlling the carrier concentration of n-type Mg₃Sb_{1.5}Bi_{0.5} compared to the chalcogen dopants.

The loss of Mg in n-type $Mg_3Sb_{1.5}Bi_{0.5}$ is a significant issue in this system that needs to be managed (with coatings, insulation or cover gas) for practical applications. Experimentally, previous studies observed that it is difficult to sustain degenerate n-type

carrier behavior at high temperature (>450 °C) in chalcogen doped samples. 1,2,14,15 We suspect the cause of this is due to different vapor pressures and reactivities of the magnesium compared to the pnictide atoms, leading to an overall loss of Mg with extended use. As stated earlier, the thermodynamic state (whether Mg-excess or Sb-excess) of Mg_3Sb_2 type compounds dramatically affects their defect formation energies and therefore the type and concentration of available charge carriers.

In addition to adjusting the carrier concentration, La substitution at the Mg site might have a substantial effect on the high temperature thermal stability of the ${\rm Mg_3Sb_{1.5}Bi_{0.5}}$ alloy. A small amount of La substitution for Yb in ${\rm Yb_{14}MnSb_{11}}$ has been shown to increase the melting point and reduce the material's overall sublimation rate by changing the bonding character to be more ionic.²²

We successfully synthesized n-type $Mg_3Sb_{1.5}Bi_{0.5}$ with Ladoping and quantitatively evaluated the thermoelectric properties of the material. La-doping is not only effective for realizing n-type conduction but it also shows higher doping efficiency for n-type $Mg_3Sb_{1.5}Bi_{0.5}$ compared to chalcogen dopants. Furthermore, improved thermal stability in the Ladoped samples was observed with less change in carrier concentration when placed in a dynamic vacuum at elevated temperature.

La-doping in the ${\rm Mg_3Sb_2-Mg_3Bi_2}$ alloy system realizes n-type conduction, with the carrier concentration of this material ranging from $\sim\!2.0\times10^{19}~{\rm cm}^{-3}$ to $\sim\!6\times10^{19}~{\rm cm}^{-3}$ by changing the nominal La concentration (Fig. 1). Compared to other chalcogen doping, the doping efficiency is higher in the cation-doped material which is consistent with the calculation of the defect formation energy. This is plainly seen when comparing samples with the same nominal concentration of dopant, with La = 0.01 achieving $n_{\rm H} = \sim\!5.5\times10^{19}~{\rm cm}^{-3}$ and Te = 0.01

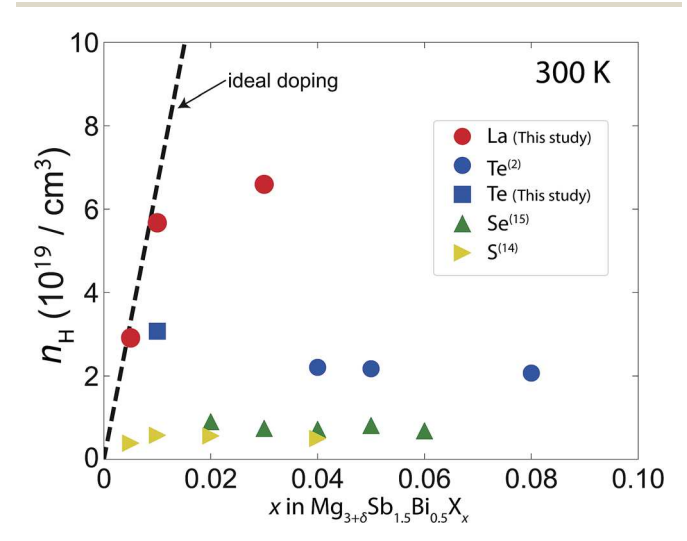


Fig. 1 The doping efficiency of ${\rm Mg_{3+\delta}Sb_{1.5}Bi_{0.5}}$ with La and chalcogen dopants (Te,² Se,¹⁵ S¹⁴) at 300 K compared to ideal doping (dotted line) calculated based on nominal composition by assuming every dopant donates a carrier. La shows higher doping efficiency compared to chalcogen dopants. Excess Mg (δ) is added to ensure n-type conduction.

achieving $n_{\rm H} = \sim 3 \times 10^{19} \ {\rm cm}^{-3}$ (Fig S1†). The nominal doping efficiency was calculated by taking the ratio of the Hall carrier concentration to the carrier concentration one would assume if all of the dopant atoms were to donate 1 electron as a charge carrier (Table 1). The ideally doped carrier concentration was estimated by taking the nominal number of dopant atoms divided by the volume of the compound. We see that La has a doping efficiency roughly double that of Te at similar concentrations, as shown in Table 1. At high levels of La, the doping efficiency begins to decrease, hinting that a solubility limit may have been reached. This increase offered by cation doping opens the door for better tuning of the electronic properties and potentially reduces impurity phases that would have formed from the excess dopant.

The thermoelectric figure-of-merit, zT = 1.0 at 600 K, is achieved in the La-doped n-type Mg₃Sb_{1.5}Bi_{0.5}. The transport properties (Fig. 2) of $La_xMg_{3.05}Sb_{1.5}Bi_{0.5}$ (x = 0.005-0.03) exhibit large values of thermopower, indicating typical behavior of degenerate semiconductors. The change in the Seebeck coefficient and electrical conductivity is consistent with the change in the carrier concentration. The thermally-activated conductivity between 300 and 500 K can be attributed to the high resistive grain boundary region.^{23,24} The different scattering mechanisms cannot mathematically explain the drastic crossover of conductivity from the trend of $T^{1.5}$ to $T^{-1.5}$ within 300-600 K. (See the ESI of ref. 23). Improved low temperature conductivity in x = 0.03 suggests that La doping affects both the bulk Fermi level and the grain boundary chemistry.23 Among our samples with different La content, the sample with the La content x =0.005 gives the highest thermoelectric performance with zT =1.0 at 600 K (Fig. 2).

A material's figure of merit (zT) is strongly dependent on its carrier concentration as its electrical conductivity, Seebeck coefficient, and electronic portion of thermal conductivity are all functions of the Fermi level. Therefore, the dimensionless materials quality factor B was introduced as a fundamental material property not dependent on the Fermi level or carrier concentration. ^{25,26} The material's quality factor B is defined by the following equation. ^{25,26}

$$B = \left(\frac{k_{\rm B}}{e}\right)^2 \frac{e(2m_{\rm e}k_{\rm B}T)^{3/2}}{3\pi^2\hbar^3} \frac{\mu_{\rm W}}{\kappa_{\rm L}} T \tag{1}$$

In this regime, we can evaluate the electrical properties and the thermal properties separately as the weighted mobility μ_W and the lattice thermal conductivity κ_L .

The weighted mobility for each sample is calculated from experimental thermopower and electrical conductivity. 26,27 The temperature dependency of the calculated weighted mobilities for La-doped (La content x = 0.005, 0.01, 0.03) and Te doped (Te content 0.01) samples is shown in Fig. 3a. From this study, it appears that La doping decreases the intrinsic mobility compared to Te doping. Fig. 3b shows a Pisarenko plot (Seebeck coefficient ν s. Hall carrier concentration) at 300 K in which a single parabolic band mass of $1.2m_{\rm e}$ agrees well with both Te doped and La doped samples. This indicates that, at least at

46%

 $X_x = Te_{0.01}$

Hall carrier concentration Ideal doping carrier $(10^{19} \text{ cm}^{-3})$ concentration (1019 cm-3) $Mg_{3.05}Sb_{1.5}Bi_{.05}X_x$ Doping efficiency $X_x = La_{0.005}$ 2.91 88% 3.30 $X_x = La_{0.01}$ 5.67 6.60 86% $X_x = La_{0.03}$ 6.59 19.8 33%

6.60

Table 1 Hall carrier concentration at 300 K compared to the ideally doped samples' carrier concentrations

room temperature, the band structure of the conduction band is not significantly changed by doping with La instead of Te.

3.07

To evaluate the change in thermal properties with La-doping, the lattice thermal conductivity, $\kappa_{\rm L} = \kappa_{\rm tot} - \kappa_{\rm e}$, was obtained by calculating κ_e using the Wiedeman–Frantz law, $\kappa_e = LT/\rho$, where L is the Lorentz number. Assuming acoustic phonon scattering and a single parabolic band model, the Lorentz number was determined using the experimental Seebeck coefficient.²⁷ It was noted that the electrical contribution to thermal conductivity can be estimated using the bulk Lorenz number as the Fermi level calculated from the Seebeck coefficient mainly reflects the bulk properties. In this method, all the inhomogeneous factors introduced by grain boundary scattering can be approximated to the first order using the conductivity. The calculated lattice thermal conductivities of samples with different La content (x =0.005, 0.01, 0.03) and a sample with a Te content of 0.01 are shown in Fig. 3c. Although we can expect some reduction in lattice thermal conductivity by alloying with heavier elements,28-31 we do not observe a significant difference in the lattice thermal conductivities between the La- and Te-doped samples. This is likely because the amount of dopant is too small to meaningfully change the phonon scattering. The x =0.03 sample possesses slightly higher lattice thermal conductivity compared to other samples, which might be attributed to the existence of an impurity phase that has higher thermal conductivity and a relatively large amount of La as reported in a previous report with different amounts of excess Mg.13 Although this is implied in the decrease in doping efficiency, we could not find a signal for any impurity phase in the XRD results (see Fig. S2†) since the nominal amount of La is too small to detect.

The quality factor of this material was calculated to be 0.45 at 600 K, which predicts that $zT = \sim 1.1$ when the material is optimized in terms of carrier concentration. This predicted zThas almost the same value as that of our best sample (La content x = 0.005), as seen in the predicted value of zT from the carrier concentration plot (Fig. 3d), which shows that this sample carrier concentration is effectively optimized. The quality factor

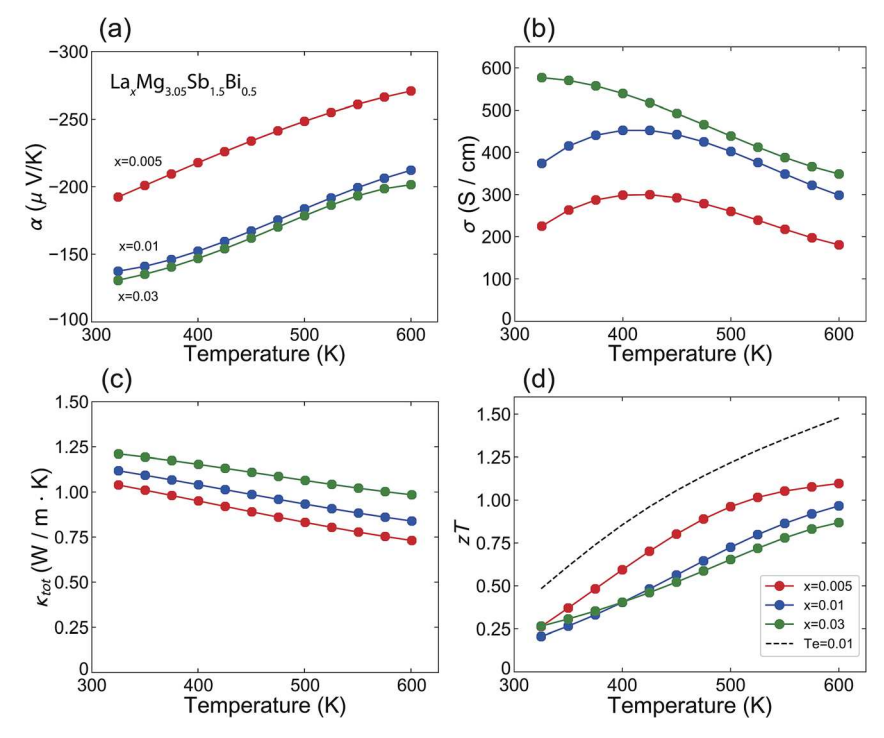


Fig. 2 Transport properties of $La_xMg_{3.05}Sb_{1.5}Bi_{0.5}$ (x=0.005-0.03) as a function of temperature: (a) Seebeck coefficient α ; (b) electrical conductivity σ ; (c) total thermal conductivity κ_{tot} ; (d) figure-of-merit $zT = (\alpha^2 \sigma)T/\kappa$. The change in transport properties is consistent with carrier concentration change.

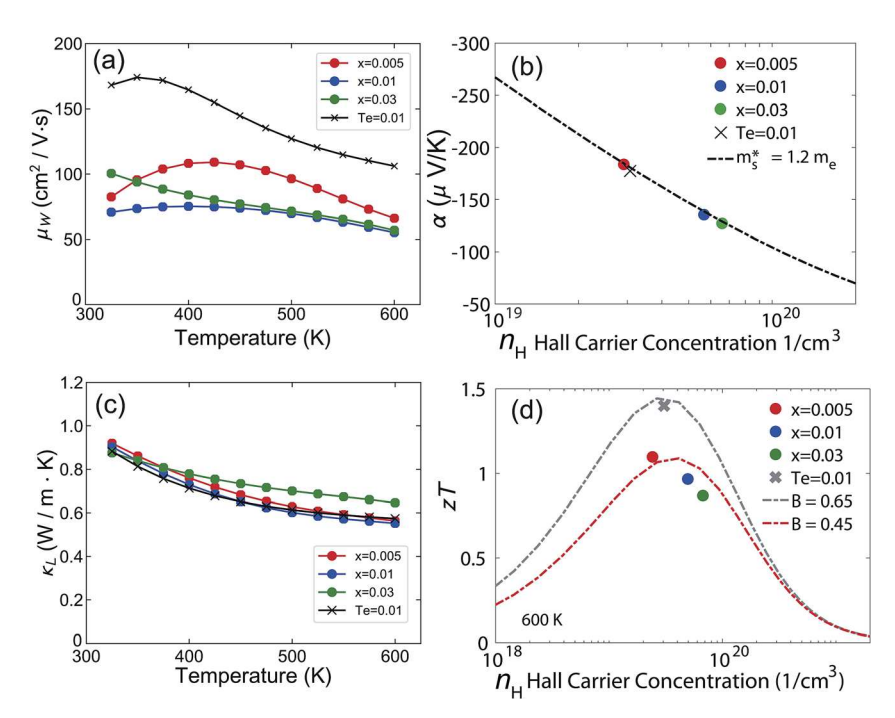


Fig. 3 (a) Weighted mobility, (b) Pisarenko plot at 300 K, (c) lattice thermal conductivity and (d) zTvs. Hall carrier concentration plots at 600 K for $La_xMg_{3.05}Sb_{1.5}Bi_{0.5}$ (x=0.005-0.03) and $Mg_{3.05}Sb_{1.5}Bi_{0.5}Te_{0.01}$.

of the La-doped sample is smaller than that of the Te-doped sample, which is due to its smaller weighted mobility. Some of this decrease in mobility is likely attributed to the perturbation of the periodic potential at the conduction band due to the cation site doping by La,²¹ but could also be related to impurity phases that vary with processing conditions.

We have conducted Hall measurements under dynamic vacuum for both a Te-doped and La-doped sample for 72 hours under identical conditions. The goal of this was to see the

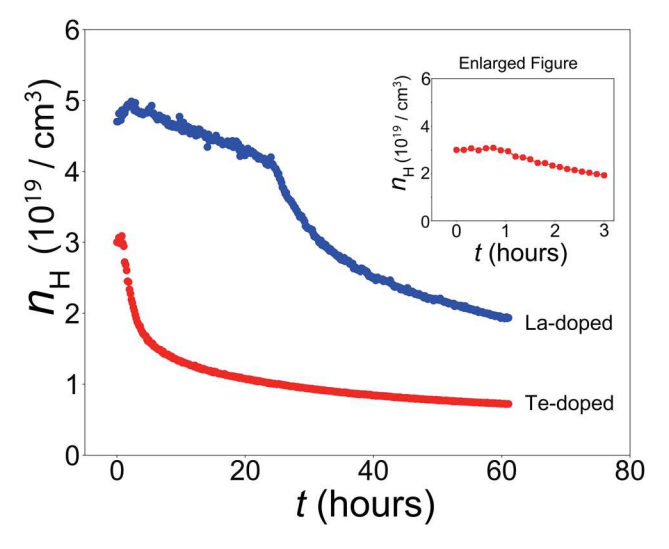


Fig. 4 Time dependency of the Hall carrier concentration of the Ladoped sample $(La_{0.01}Mg_{3.05}Sb_{1.5}Bi_{0.5})$ and the Te-doped sample $(Mg_{3.05}Sb_{1.5}Bi_{0.5}Te_{0.01})$ measured in a dynamic vacuum that removes Mg vapor.

change in Hall carrier concentration as a function of time at the elevated temperature of 450 °C, the results of which are seen in Fig. 4. Both samples exhibit a linear decrease followed by an exponential decrease (in log y scale) in Hall carrier concentration. The Te-doped sample only exhibits a linear decrease in Hall carrier concentration for 1 hour and then exponentially decreases such that within 20 hours, the carrier concentration of the Te sample decreased by more than 65% and reaches below $n_{\rm H} = 1 \times 10^{19} \ {\rm cm}^{-3}$. The La-doped sample shows a slow linear decrease for approximately 25 hours, then begins an exponential type decay. The decrease in this linear region is only about 17% which is much lower than the decrease of 65% in the Te-doped sample. Additionally, over the whole period of measurement the La-doped sample loses 62% of its carriers compared to 80% in the Te doped sample. Finally, we would like to note that this material has an optimized carrier concentration in the $2-5 \times 10^{19} \ \text{cm}^{-3}$ range (Fig. 3d). At the end of the measurement the La-doped sample had a carrier concentration of 1.9×10^{19} cm⁻³, whereas the Te doped sample had a carrier concentration of $7.2 \times 10^{18} \text{ cm}^{-3}$.

The exponential change in carrier concentration over time at elevated temperatures in these samples is likely related to the Mg content present in the samples. In a dynamic vacuum, the excess Mg needed to suppress the formation of electron compensating Mg vacancies³ slowly decreases due a net loss of Mg. During the regime where there is a slow, linear decrease in Hall carrier concentration, the dopant itself may also be evaporating or its doping efficiency decreasing. However when the Mg evaporation causes the sample to reach the nominal composition where the thermodynamic state is no longer Mg-excess, a dramatic change in carrier concentration will occur.

Starting at the surface, the material will become p-type, leading to the exponential drop in Hall carrier concentration.

Communication

We suspect that cation doping changes the defect energetics in the sample in such a way that it suppresses the net loss of Mg, which results in the improvement of the thermal stability at high temperature as also reported in the 14-1-11 system.²² Therefore, we can conclude that La-doping significantly improves the thermal stability of n-type Mg_{3.05}Sb_{1.5}Bi_{0.5}, thus, cation-doping can be a more realistic strategy to put this material into practice as thermoelectric generators for applications such as waste heat recovery technology and deep space power generation. Also, we would like to note that the improved thermal stability might also allow the hot pressing of this material at higher temperature. Larger grain size with higher pressing temperature is a useful method to get better electrical performance, especially for low temperatures, by reducing grain boundary resistance.23,24

In conclusion, cation-site doping using La for n-type Mg_{3.05}Sb_{1.5}Bi_{0.5} shows higher doping efficiency than anionsite chalcogen doping. An optimized zT > 1.0 at 600 K was achieved with a La content x = 0.005 in La_xMg_{3.05}Sb_{1.5}Bi_{0.5}. Enhanced thermal stability of n-type Mg_{3,05}Sb_{1,5}Bi_{0,5} was observed with La doping. In a long term measurement at the elevated temperature of 450 °C, degenerate n-type conduction in the La doped sample lasts far longer than in the Te-doped sample. While the intrinsic mobility appears to be lower in Ladoped samples compared to that of anion-doped samples, the higher processing temperatures enabled by the enhanced thermal stability may enable future improvements in mobility using optimized processing conditions.

Experimental section

La_xMg_{3.05}Sb_{1.5}Bi_{0.5} was synthesized with different nominal values of La (x = 0.005-0.3). In addition to these samples, one sample with Te doping was also synthesized using the same procedure with a composition of Mg_{3.05}Sb_{1.5}Bi_{0.5}Te_{0.01}. We sealed magnesium turnings (99.98%, Alfa Aesar), antimony shots (99.9999%, 5N Plus), bismuth granules (99.999%, 5N Plus), lanthanum lumps (99.999%, Alfa Aesar), and Te shots (99.999%, 5N Plus) into stainless steel vials according to the nominal compositions in an argon-filled glove box. The elements were mechanically alloyed using high-energy ball milling with a high-energy mill (SPEX 8000D) for two hours. The processed powder was loaded into a graphite die and pressed using an induction heating rapid hot press for 20 minutes at 1073 K and 45 MPa under an argon gas flow.32 The Seebeck coefficient of each sample was measured with chromel-Nb thermocouples in a two-probe configuration under a dynamic high vacuum.33 The Hall coefficient and electric resistivity were measured simultaneously using a 4-point probe Van der Pauw technique with a 2 T magnetic field under a dynamic high vacuum. Thermal diffusivity D was measured using a flash method with a Netzsch LFA 457 under a flowing argon atmosphere. The thermal conductivity κ was calculated using $\kappa = D \times D$ $C_p \times d$, where d is density and C_p is heat capacity (see the ESI[†] for C_p data³⁴). The thermal stability of the materials was

measured via the change in the Hall carrier concentration over an extended time at an elevated temperature. With the same set up as the above-mentioned Hall system, we measured the Hall coefficient and resistivity for 72 hours for both La_{0.01}Mg_{3.05}- $Sb_{1.5}Bi_{0.5}$ and $Mg_{3.05}Sb_{1.5}Bi_{0.5}Te_{0.01}$ under a dynamic vacuum at a constant temperature ~ 450 K. Great care was taken to make sure as many experimental details as possible remained identical for both samples, such as measuring them at the same time and polishing them to an identical thickness of 1 mm. We should note that the Hall stage in our set up is made of alumina, which can potentially react with Mg at elevated temperatures.

Conflicts of interest

There are no conflicts to declare.

Acknowledgements

This work was supported by the NASA Science Mission Directorate's Radioisotope Power Systems Thermoelectric Technology Development and the Solid-State Solar-Thermal Energy Conversion Center (S3TEC), an Energy Frontier Research Center funded by the U.S. Department of Energy, Office of Science, Basic Energy Sciences under Award # DE-SC0001299. The IMSERC X-ray Facility at Northwestern University is supported by the Soft and Hybrid Nanotechnology Experimental (SHyNE) Resource (NSF ECCS-1542205); the State of Illinois and International Institute for Nanotechnology (IIN).

References

- 1 H. Tamaki, H. K. Sato and T. Kanno, Adv. Mater., 2016, 28, 10182-10187.
- 2 J. Zhang, L. Song, S. H. Pedersen, H. Yin, L. T. Hung and B. B. Iversen, Nat. Commun., 2017, 8, 13901.
- 3 S. Ohno, K. Imasato, S. Anand, H. Tamaki, S. D. Kang, P. Gorai, H. K. Sato, E. S. Toberer, T. Kanno and G. J. Snyder, Joule, 2018, 2, 141-154.
- 4 W. Peng, G. Petretto, G.-M. Rignanese, G. Hautier and A. Zevalkink, Joule, 2018, 2, 1879-1893.
- 5 V. Ponnambalam and D. T. Morelli, J. Electron. Mater., 2013, 42, 1307-1312.
- 6 H. X. Xin and X. Y. Qin, J. Phys. D: Appl. Phys., 2006, 39, 5331-
- 7 S. H. Kim, C. M. Kim, Y.-K. Hong, K. I. Sim, J. H. Kim, T. Onimaru, T. Takabatake and M.-H. Jung, Mater. Res. Express, 2015, 2, 055903.
- 8 C. L. Condron, S. M. Kauzlarich, F. Gascoin and G. J. Snyder, J. Solid State Chem., 2006, 179, 2252-2257.
- 9 J. Li, S. ZHENG, T. Fang, L. Yue, S. Zhang and G. Lu, Phys. Chem. Chem. Phys., 2018, 20, 7686-7693.
- 10 J. Shuai, J. Mao, S. Song, Q. Zhu, J. Sun, Y. Wang, R. He, J. Zhou, G. Chen, D. J. Singh, Z. Ren, C. W. Chu, G. Chen and Z. Ren, Energy Environ. Sci., 2017, 10, 799-807.
- 11 J. Shuai, J. Mao, S. Song, Q. Zhang, G. Chen and Z. Ren, Materials Today Physics, 2017, 1, 74-95.

- 12 K. Imasato, S. D. Kang, S. Ohno and G. J. Snyder, *Mater. Horiz.*, 2018, 5, 59–64.
- 13 K. Imasato, S. Ohno, S. D. Kang and G. J. Snyder, *APL Mater.*, 2018, **6**, 016106.
- 14 J. Zhang, L. Song, K. A. Borup, M. R. V. Jørgensen and B. B. Iversen, *Adv. Energy Mater.*, 2018, 1702776.
- 15 J. Zhang, L. Song, A. Mamakhel, M. R. V. Jørgensen and B. B. Iversen, *Chem. Mater.*, 2017, **29**, 5371–5383.
- 16 J. Mao, Y. Wu, S. Song, Q. Zhu, J. Shuai, Z. Liu, Y. Pei and Z. Ren, ACS Energy Lett., 2017, 2, 2245–2250.
- 17 S. Ohno, U. Aydemir, M. Amsler, J. H. Pöhls, S. Chanakian, A. Zevalkink, M. A. White, S. K. Bux, C. Wolverton and G. J. Snyder, *Adv. Funct. Mater.*, 2017, 27, 1606361.
- 18 J. Shuai, B. Ge, J. Mao, S. Song, Y. Wang and Z. Ren, *J. Am. Chem. Soc.*, 2018, **140**, 1910–1915.
- 19 L. R. Jørgensen, J. Zhang, C. Zeuthen and B. B. Iversen, *J. Mater. Chem. A*, 2018, **6**, 17171–17176.
- 20 P. Gorai, B. R. Ortiz, E. S. Toberer and V. Stevanović, *J. Mater. Chem. A*, 2018, **6**, 13806–13815.
- 21 H. Wang, X. Cao, Y. Takagiwa and G. J. Snyder, *Mater. Horiz.*, 2015, 2, 323–329.
- 22 I. G. Vasilyeva, R. E. Nikolaev, M. N. Abdusaljamova and S. M. Kauzlarich, *J. Mater. Chem. C*, 2016, 4, 3342–3348.
- 23 J. J. Kuo, S. D. Kang, K. Imasato, H. Tamaki, S. Ohno, T. Kanno and G. J. Snyder, *Energy Environ. Sci.*, 2018, **11**, 429–434.

- 24 T. Kanno, H. Tamaki, H. K. Sato, S. D. Kang, S. Ohno, K. Imasato, J. J. Kuo, G. J. Snyder and Y. Miyazaki, *Appl. Phys. Lett.*, 2018, **112**, 033903.
- 25 R. P. Chasmar and R. Stratton, *J. Electron. Control*, 1959, 7, 52–72.
- 26 S. Dongmin Kang and G. Jeffrey Snyder, *Nat. Mater.*, 2016, 16, 252-257.
- 27 A. F. May and G. J. Snyder, in *Materials, Preparation, and Characterization in Thermoelectrics*, ed. D. M. Rowe, CRC Press, 2012, pp. 1–18.
- 28 F. Gascoin, S. Ottensmann, D. Stark, S. M. Haïle and G. J. Snyder, *Adv. Funct. Mater.*, 2005, **15**, 1860–1864.
- 29 X. Shi, Y. Pei and D. T. Morelli, Appl. Phys. Lett., 2009, 94, 122112.
- 30 H. Wang, A. D. Lalonde, Y. Pei and G. J. Snyder, Adv. Funct. Mater., 2013, 23, 1586–1596.
- 31 J. Yang, G. P. Meisner and L. Chen, *Appl. Phys. Lett.*, 2004, **85**, 1140–1142.
- 32 A. D. LaLonde, T. Ikeda and G. J. Snyder, *Rev. Sci. Instrum.*, 2011, **82**, 025104.
- 33 S. Iwanaga, E. S. Toberer, A. Lalonde and G. J. Snyder, *Rev. Sci. Instrum.*, 2011, **82**, 063905.
- 34 M. T. Agne, K. Imasato, S. Anand, K. Lee, S. K. Bux, A. J. E. Rettie, D. Y. Chung, M. G. Kanatzidis and G. J. Snyder, *Mater. Today Phys.*, 2018, DOI: 10.1016/ j.mtphys.2018.10.001.